

Experimental results from the optical planet detector interferometer

J. Kent Wallace, M. Shao, B. Lane, B. M. Levine, F. Loya, A. Azizi, Buck Holmes,
F. Aguayo, J. Negron, G. Sanchez, Robert Gappinger
Jet Propulsion Laboratory, California Institute of Technology
4800 Oak Grove Dr.
Pasadena, CA USA 91105

ABSTRACT

Researches have suggested several techniques (ie.: pupil masking, coronagraphy, nulling interferometry) for high contrast imaging that permit the direct detection and characterization of extrasolar planets. Our team at JPL, in previous papers^{1,3}, has described an instrument that will combine the best of several of these techniques: a single aperture visible nulling coronagraph. The elegant simplicity of this design enables a powerful planet-imaging instrument at modest cost. The heart of this instrument is the visible light nulling interferometer for producing deep, achromatic nulls over a wide optical band pass, and a coherent array of single mode optical fibers² that is key to suppressing the level of scattered light. Both of these key components are currently being developed and have produced initial results. This paper will review, in detail, the design of the nulling interferometer experiment and review the latest experimental results. These results illustrate that we are well on our way to developing the fundamental components necessary for planned mission. Likewise, our results demonstrate that the current nulling levels are already consistent with final requirements.

Keywords: space-based stellar interferometry, coronagraphy, nulling interferometry, extrasolar planets

1. INTRODUCTION

Broadband nulling interferometry necessarily requires the electric field vectors from two separate arms of an interferometer to be exactly opposite in orientation for all wavelengths at the point of recombination. This is easy to say, and it is altogether a much more difficult thing to demonstrate experimentally. Initial experiments, insightful as they were, led us to the conclusion that the task of nulling is more easily accomplished by splitting the task into two major components: first, an achromatic fields flip and second a fully symmetric beam combiner. Likewise, our initial techniques for controlling the null suffered from the need to dither the null, thereby limiting the achievable null depth.

The shearing interferometer for this experiment benefits from all of our previous nulling attempts. In the next section the experiment will be described in detail, from the source input to the interferometer output, including the laser metrology and a brief discussion of the control algorithm and hardware. Afterwards, we'll present and discuss some of the recent experimental results. To conclude, we will briefly discuss our future plans for the testbed.

2. INSTRUMENT DESCRIPTION

2.1 Primary interferometer functions

The task of the interferometer can be summarized by its few key functions: phasing, shearing, and field flipping. For reference, a layout of the interferometer is shown in figure 1. For simplicity of implementation, we choose one arm of the interferometer to perform the task of phasing. Its task is simply to maintain the differential air path between the two arms to be very nearly zero. This path can be positioned accurately (to within a few tenths of a nanometer) and maintained for long periods of time (tens of seconds) with laser metrology. Shear is accomplished with the other arm of the interferometer. The rooftop in this arm of the interferometer can move, coarsely, transverse to the beam direction. There is a sub-aperture on the output of the interferometer that selects the overlap region of the sheared beams. In this way, it's possible to create an adjustable, short baseline interferometer when this subaperture is projected back to the input aperture. Field flip is accomplished by the use of a combination of glass plates of differential thickness and air delay to create a pseudo-achromatic pi phase change⁴. This technique was deemed advantageous, for although it's possible to create a broadband achromatic field flip with the correct implementation of reflecting mirrors⁵ (including an out-of-plane reflection), this 'geometric' field flip also results in a flip of the input pupil. This 'pupil flip' creates a double image of the field in the final focal plane (the second

image is inverted about the optical axis of the system). This can lead to an ambiguity as to the true location of the planet relative to the star. Also, use of the phase plates produces a very compact, in-plane system.

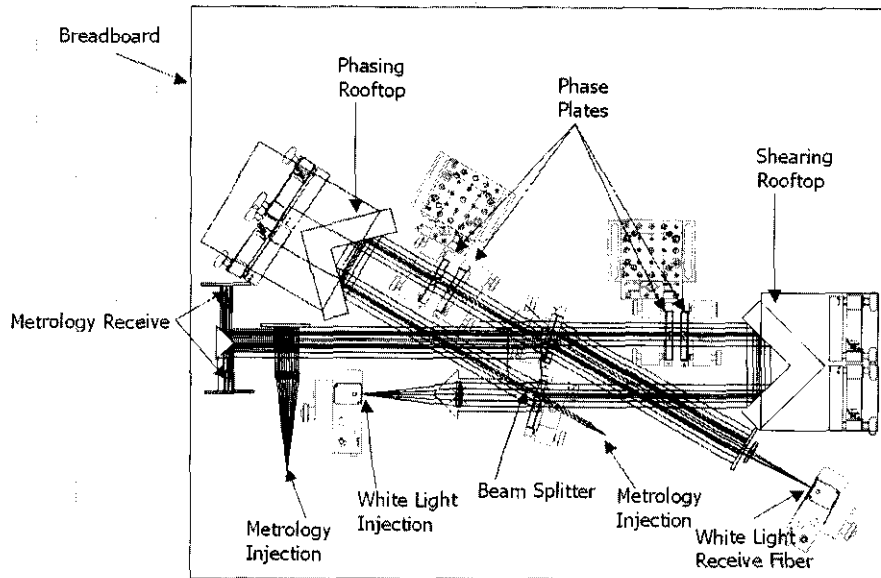


Figure 1. Layout of the nulling interferometer. The source is located on the left-hand side of the experiment. The output to a single mode optical fiber is on the lower right. Metrology injection occurs on the backside opposite side of the main beamsplitter as the white light injection. The local oscillator is on the 'bright' output as well as the metrology receivers. The dimensions of the breadboard are 23"x28".

2.2 Description of the system

First, several steps have been taken to insure that the experiment is located in a moderately quiescent environment. It is located on a ~2'x2.5' breadboard that is supported upon an 4'x6' optical table with sorbothane pucks. These pucks provide passive damping of mechanical vibrations. The optical table is then covered with a Plexiglas enclosure that is lined with insulating foam. The enclosure helps to dampen the air currents and minimize acoustic coupling. Two-inch thick black foam lines the inside of this enclosure, thereby providing another layer of mechanical, thermal, and acoustic isolation. The optical table has pneumatic isolation legs that provide another layer of isolation from mechanical disturbances. All cables (optical fibers, electrical connectors) that feed the instrument are strain-relieved to minimize mechanical coupling of vibrations.

2.2.1 Source

Referring to figure 1, the source which feeds the interferometer is a single mode fiber (cut-off wavelength of 590 nm). This can be fed with any number of optical sources. The two primary ones are a laser diode and a filtered, thermal white light source. Using a single mode fiber as a source allows us to quickly and easily change sources without disturbing the internal alignment of the system. The source is collimated with an achromatic doublet that provides a well collimated beam over a broad optical band.

2.2.2 Beamsplitters

The custom beamsplitters were designed and implemented to work with a small angle of incidence (~15 degrees). The motivation for designing them for this angle of incidence was to minimize the effect of polarization dispersion. As the angle of incidence increases on an uncoated substrate, the effect on the phase and amplitude of the reflected light of both polarizations starts to diverge. (At Brewster's angle for instance, there is no reflected 's' polarization.) Although the effect for a multilayer optical coating can be made much different from the properties of a bare surface, one thing is sure: at normal incidence the properties of the coating are identical for s and p, so the polarization dispersion is zero. For this reason, we try to stay as close to zero angle of incidence as physically possible.

2.2.3 Rooftops

Currently, each rooftop is made from two separate pieces of two-inch square gold-coated mirrors. Each rooftop is aligned interferometrically in front of a Zygo phase-shifting interferometer to within a few arc seconds. In the phasing arm of the interferometer, one of the mirrors is attached to a PZT flexure stage that provides very precise position control (0.1 nm) and very low angular runout over the full range of the motion (15 μ m).

2.2.4 Shutters

Electronic shutters in each arm of the interferometer allow us to easily monitor the intensity. The shutters are normally open, and therefore only draw current when they are closed. This allows us to keep the thermal load internal to the experiment at a minimum.

2.2.5 Interferometer Output

Light is interfered at the recombination beamsplitter and then fed to a single mode output fiber⁸ via an achromatic doublet. A single mode fiber optic splitter in the ratio of 99/1 is employed to divide the light between a very sensitive control detector and a high dynamic range optical power meter. The location of the output fiber in the focal plane can be adjusted in two orthogonal axes within about 20 nm.

2.2.6 Laser Metrology

Relative laser metrology gauge is used to actively monitor the optical path length internal to the interferometer. The beams are smaller than the white light beams (about 2 mm) and are nominally centered on the source beam. The measurement beam is s polarized, and is injected into the system from the opposite side of the main beam splitter. This light then traverses the interferometer and is recombined at the second beamsplitter. Here the beams are spatially separated with respect to each other by the amount of the shear. These two beams exit the interferometer on the opposite side of the interferometer as the input light. Each beam is combined with a 'local oscillator' beam, of p polarization, that spatially overlaps both beams at the polarization beamsplitting cube. A right angle prism that is silver coated on the external edges is used to redirect each beam through a linear polarizer at 45 degrees (to mix the s and p polarization states) and onto a detector. The metrology wavelength is 1319 nm, well beyond the optical band of interest, such that it does not interfere with the optical detectors. The metrology beams are fed to the interferometer using polarization maintaining single mode optical fibers. This makes for a clean and simple interface to the experiment. A half-wave plate located on the laser source plate allows us to adjust the balance of optical power between the s and p polarization states so as to improve the metrology signal contrast.

Signals from the metrology detectors (pre-amps) are then fed to 'post-amps' that perform several functions: 1) they remove the DC offset, 2) amplify the input signal, and 3) converts the sine wave inputs to square waves on the output. Care was taken to insure that both the pre-amps of the post-amp used the same power supply, thereby minimizing the effect of ground loops. These signals are then sent to the phase-meter cards that determine the phase of the input signals relative to each other with high precision. These phase meter cards provide a raw metrology measurement at 100kHz as well as on board averaging of the measured phase signal at 1kHz. Data from the phase meter card is sent from the VME bus to the PCI bus of the host computer via a fiber-coupled VME to PCI bridge.

2.2.7 Control System

Experiment control, and data acquisition is accomplished via a dual processor PC. All real-time related tasks are dedicated to one CPU, all functions related to the operating system, gui and data archiving are relegated to the other CPU. In this manner, we can be guaranteed the high performance of a truly deterministic real-time environment while also benefiting from the readily available, off-the shelf software that perform the less demanding tasks. Our real-time OS is RTX. Interfaces and requests to the real-time system are made via ActiveX calls from the system OS. This setup is very robust, easy to maintain, completely sufficient for our modest needs, and relatively modest in cost.

3. EXPERIMENTAL OBSERVATIONS

3.1 Observation Preliminaries

Before each nulling observation is made, we check a few metrics to insure that the null test will be a good one. The first critical contributor is the intensity balance in each arm. An imbalance in the intensity between the two arms of $\delta I = \Delta I/I$, results in a limiting null depth of $N = \delta I^2/4$. For a null depth of a 500K:1, the corresponding intensity match must be <0.28%. In order to accommodate this level of balance, we shutter each arm in the interferometer,

measure the average over 400 seconds, and compare the two. If there is a mismatch in the intensity, the location of the output fiber is adjusted, ever so slightly, to a point where the balance matches the criteria.

The second driving factor in determining the null depth is the fluctuation of path length. Null depth, if residual path length fluctuation is the only contributing factor, is given by: $N = \Delta\phi^2/4$ (where $\Delta\phi$ is in radians). The operating wavelength of our interferometer is 635 nm and the required rms pathlength fluctuations for a null of 200K:1 is 0.224 nm.

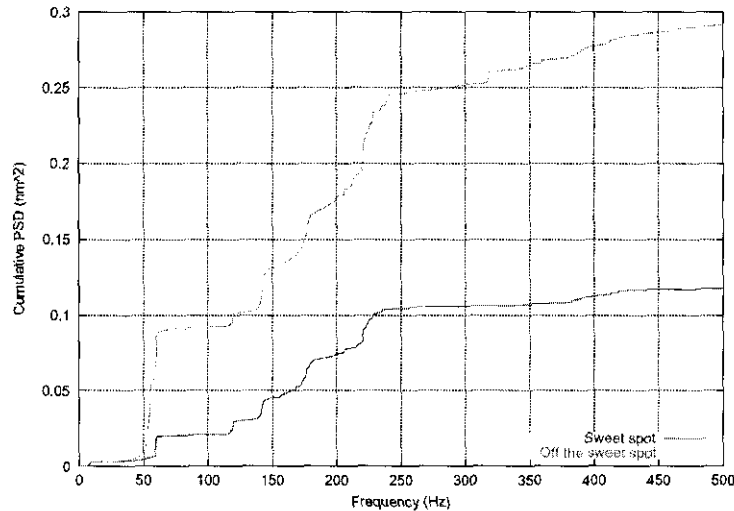


Figure 2. Cumulative power spectral density of path length fluctuations as measured by laser metrology. For a null depth of 200K:1, the rms path length fluctuations must be 0.23 nm for a wavelength of 635 nm. Notice the steps at 60 and 120 Hz. The slow upward trend between 150 and 230 Hz is thought to be due to residual atmospheric fluctuations. This data was taken with the control system running.

Figure 2, above, shows a the cumulative power spectral density of the interferometer path length fluctuations while the system is in closed loop operation. Integrated out to 500 Hz, path length fluctuations are 0.13 nm which corresponds with an equivalent null depth of roughly 80K:1. The value for the residual path length fluctuations is strongly dependent upon the time of day, and the activity both in the lab, and in the surrounding areas. The GUI on the experiment has a real time display of the RMS path length fluctuations, so it's easy to determine the level to which the nulling will be set by these fluctuations. Indeed, this is using the metrology as a most basic metric of experimental conditions. As shown in figure 2, the data encapsulated by a time sequence of the metrology makes it a powerful tool for diagnosing at just what frequency the major path length contributors occur. It's usefulness as a tool for nulling interferometer is to be appreciated.

3.2 Laser-Diode Results

After first balancing the intensity in both arms, and measuring path length fluctuations, the final step is phasing of the system. The fringe scanned manually to determine the location of the deepest laser null. Once there, the laser metrology is reset to zero, and a dither is applied to scan over the fringe. Slight asymmetries at the bottom of the dithered fringe are corrected by manual offsets to the metrology set point. Once this is set point is optimized by eye, the laser metrology is then locked to this set point and data is recorded with the optical power meter. Giving a new metrology set point easily changes the path length, and hence, the fringe contrast. Using the metrology in this way makes turning the null fringe "on" and "off" a trivial matter. Figure 3 below shows our best nulling measurement with a laser diode as the source. The path length is stabilized using the technique just described. A polarizer in the beam allows us to select the polarization state, this gives us a somewhat better null than without the polarizer which we think is due primarily to the alignment of the open face rooftop mirrors.

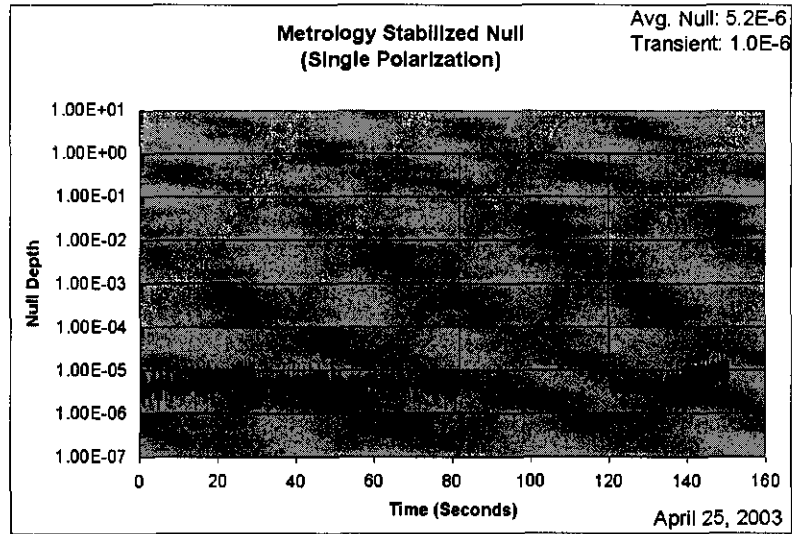


Figure 3. Nulling of a single polarization, visible laser diode (635 nm) while using laser metrology (1319 nm) to stabilize the optical path.

3.2 Preliminary white light work: FTS results

As we start development of the white part of the experiment, one of the most challenging aspects is setting the phase plates to give us a pi phase change over the optical bandwidth of interest. The addition of laser metrology into the interferometer gives us the ability to accurately measure fringe contrast as the path length changes. This data can be then be inverted using the technique of Fourier Transform Spectroscopy⁹ to give a measure of the residual phase in the system. One can then quickly imagine an iterative routine whereby the fringe is scanned, the phase determined, and a change to the glass thickness is calculated to improve the phase, and so on. We have yet to include the glass in each arm that will give us the necessary dispersion, so at this point we can simply solve for the residual dispersion due to the differential glass thickness in the beamsplitters. Figure 4 below illustrates this technique with a scan of the white light fringe and the subsequently inverted phase as a function of wavelength. A differential glass thickness required to give the phase difference was fit to the data and was determined to be 3.6 microns +/- 40 nm.

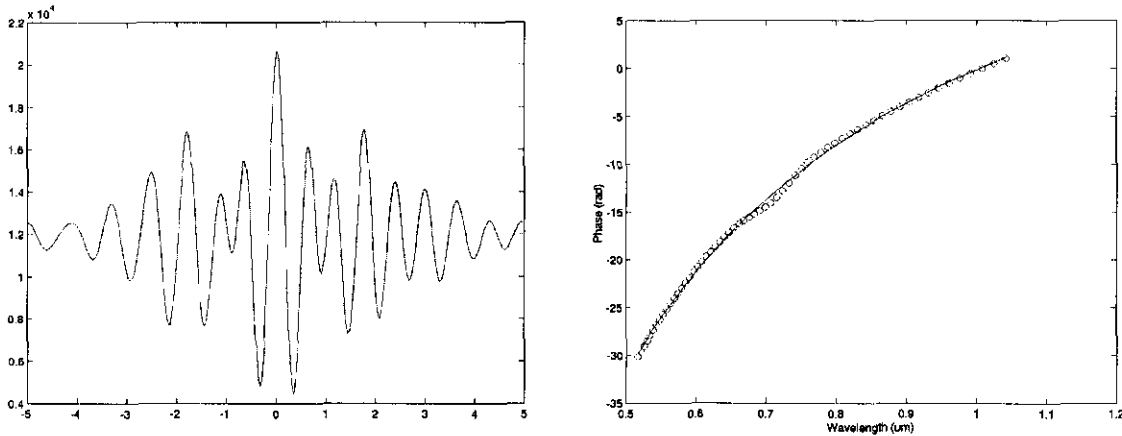


Figure 4. White light fringe scan used to determine the residual dispersion in the system.

The foundation work for implementing this technique for determining the differential glass thickness had thus been established.

4. FUTURE WORK

4.1 White light work: Single-glass phase plates

Our near term goals are do initiate white light nulling with a modest bandpass (10%) and modest nulls (10-4). It's possible to accomplish these with a differential thickness of only a single glass and a corresponding path delay in air. Figure 6, below, show a solution with a differential glass thickness of 20.006 microns on fused silica in one arm of the interferometer that is balanced by 29.465 microns of air in the other arm. The average null across optical band from 640 nm to 710 nm is 5.4×10^{-6} (~200K:1). (This glass was chosen because it is the same material as the beamsplitter substrate so we can also take out this differential glass thickness.) These phase plates are likewise in hand, and we are in the process of implementing them in the experiment. They are nominally of the equal thickness (about 0.25" thick), and we will introduce the thickness difference by giving a small angular rotation (about 6 degrees) one relative to the other. Preliminary tolerance work indicates that this can be done with modest effort (0.1 degree).

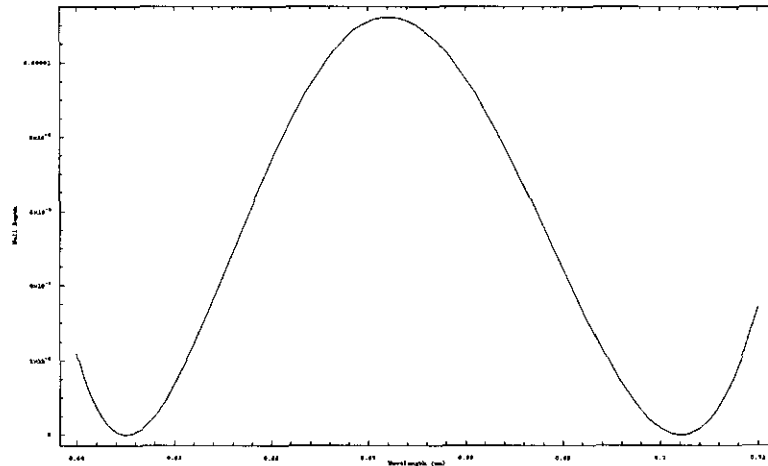


Figure 5. A solution for deep nulls using only a single, differential glass thickness and corresponding air delay is shown above. The average null depth over the band for this solution is ~200K:1.

4.2 Vacuum Chamber

The current experiment is in an open air environment. As mentioned previously, some steps have been taken to alleviate the deleterious effects of air turbulence. Indeed, the major task of the closed-loop system is to remove effects that are due primarily to fluctuations in path length due primarily to air. Therefore, in order to free ourselves of these problem, and to lighten the load of the active control system, we are working towards vacuum operation of the experiment. Figure 7 is a photo of the vacuum chamber that we've acquired and retrofitted in order to meet our requirements. It has been retrofitted with electrical and optical fiber feed thrus that relay necessary sources and signals to and from the interferometer. We are in the early stages of vacuum testing, and have hope to have the system fully operational over the next couple of months.

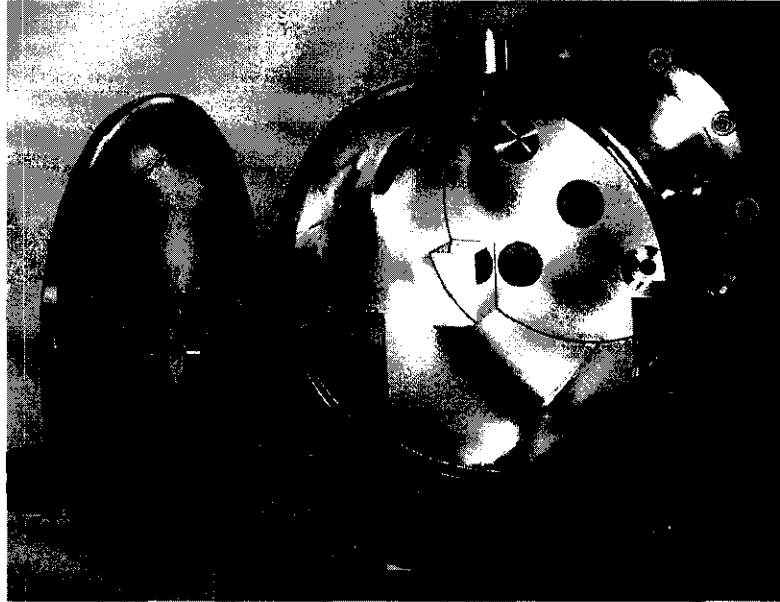


Figure. 6. The three shelves welded to the bottom interior will support the breadboard. Sorbothane isolators at these points will provide an additional amount of mechanical isolation. The flanges on the back of the chamber will be used to couple in the optical fiber components.

5. SUMMARY

We have shown experimental results from a shearing interferometer with performance that is traceable to the requirements for a proposed planet-finding mission. The novelty of this technique is the use of laser metrology to monitor the internal path-length fluctuations (a first for a nulling interferometer). We will continue to increase the optical bandpass and the null depth in order to demonstrate full technical capability.

A visible nulling coronagraph benefits from operation behind a single aperture of modest optical figure, and deep achromatic nulling with an easily adjustable baseline. This elegant yet powerful concept readily lends itself to a precursor mission with the goal of directly detecting extra-solar planets. These benefits make it a compelling idea, worthy of serious consideration.

ACKNOWLEDGEMENTS

This work was carried out by the Jet Propulsion Laboratory, California Institute of Technology, under contract with the National Aeronautics and Space Administration and supported by the Terrestrial Planet Finder Program – TPF.

REFERENCES

1. B. Mennesson, et. al., 2002, Optical Planet Discoverer: How to Turn a 1.5 m Telescope into a powerful exoplanetary systems imager, *Proc. SPIE*,
2. D. Liu, et. al. 2003, Design and fabrication of a coherent array of single-mode optical fibers for the nulling coronagraph, these proceedings.
3. M. Shao, et. al. 2003, Planet detection in visible light with a single-aperture telescope and nulling coronagraph, these proceedings.
4. R. M. Morgan, J. Burge, & N. Woolf, "Achromatic phase control using refractive materials", *Proc. SPIE* 4006, 340, 2000.
5. J. Kent Wallace, G. Hardy, and E. Serabyn, "Deep and stable interferometric nulling of broadband light with implications for observing planets around nearby star", *Nature*, **406**, 700.

6. E. Serabyn and M. Colavita, "Symmetric Beam Combiners for Nulling Interferometry, *Applied Optics*, **40**, 1668.
7. E. Serabyn, *Proc. SPIE*, 4006, 328, 2000.
8. B. Mennesson, M. Ollivier and C. Ruiller, "Single-mode waveguides to correct the optical defects of a nulling interferometer", *J. Opt. Soc. Am.*, **19**, 3, 596.
9. J. W. Brault, "Fourier Transform Spectrometry", Proc. 15th Adv. Course in Astr. & Astrophysics, Huber, Benz & Mayor, eds., (1985).